IEEE Access
Multidisciplinary | Rapid Review | Open Access Journal

Received September 18, 2018, accepted November 1, 2018. Date of publication xxxx 00, 0000, date of current version xxxx 00, 0000.

*Digital Object Identifier 10.1109/ACCESS.2018.2883378*

# Automated Application of Full Matrix Capture to Assess the Structural Integrity of Mooring Chains

**MAHESH DISSANAYAKE[1,2], (Student Member, IEEE), DAVID CARSWELL[3], MICHAEL CORSAR[2], TARIQ PERVEZ SATTAR[2], MARK SUTCLIFFE[3], PREMESH SHEHAN LOWE[3], (Member, IEEE), AND TAT-HEAN GAN[3]**

[1]School of Engineering, London South Bank University, London SE1 0AA, U.K.
[2]London South Bank Innovation Centre, Cambridge CB21 6AL, U.K.
[3]TWI Ltd., Cambridge CB21 6AL, U.K.

Corresponding author: Mahesh Dissanayake (mahesh.dissanayake@lsbu.ac.uk)

This work was supported in part by InnovateUK (RIMCAW) under Grant 102905, in part by London South Bank University, in part by TWI Ltd., Cambridge, in part by the London South Bank Innovation Centre, and in part by the National Structural Integrity Research Centre.

**ABSTRACT** In-service mooring chains are subjected to harsh environmental conditions on a daily basis, which increases the necessity of integrity assessment of chain links. Periodic structural health monitoring of mooring chains is mandatory and vital in order to maintain the safety of floating platforms. Application of ultrasound for in-service mooring chain inspection is still in its infancy due to the lack of accessibility, in-field operational complexity, and the geometrical features of mooring systems. With the advancement of robotic/automated systems (i.e., chain climbing robotic mechanisms), interest in in situ ultrasound inspection has increased. At present, ultrasound inspection has been confined to the weld area of the chain links. However, according to recent studies on fatigue and residual stresses, ultrasound inspection of the chain crown should be further investigated. A new application of ultrasonic phased array full matrix capture is discussed in this paper for investigation of the chain crown. Due to the complex geometry (i.e., curved and limited access) of the chain crown, a surface mapping technique has been added to the presented full matrix capture technique. The inspection method presented in this paper is suitable for chain links both in air and underwater. A continuous water supply wedge was developed in order to supply couplant for in-air inspection. Development of a technique that can be adapted for robotic inspection was considered, and an automated manipulator was used to carry out inspections. The design of the inspection method and the robotic manipulator is discussed in this paper. The technique is validated with laboratory experiments.

**INDEX TERMS** Mooring chain inspection, FMC algorithm, robotic inspection, mooring chain, structural health monitoring, mooring NDT (non-destructive testing), phased-array ultrasound.

## I. INTRODUCTION

With the advancement of the shipping industry, mooring chains were introduced when it became necessary to maintain a floating structure at a precise location. The exponential increase of world energy consumption has led to an increase in floating oil and gas production platforms where mooring chains are required to stabilize and hold the platform in place. Mooring chains are subjected to large tidal waves, storms, hurricanes and the corrosive effect of salt water. Therefore, it is essential to monitor the integrity of the mooring chain links. Mooring breakage can lead to significant and catastrophic events which include vessel drift, riser rupture, production shutdown and hydrocarbon spill, *etc*. For example, it cost $1.8 billion to rectify the mooring failure of the "Gryphon Alpha" production vessel in 2011 [1]. Twenty-one mooring accidents were recorded between 2001-2011 and eight of them were categorized as multiple mooring breakages [2]. Most modern systems are designed to cope with a single breakage, but multiple breakages can jeopardize the safety of the platform. According to historic data from 1920-2001, on average every 4.7 years a floating production unit/system will experience a mooring failure [3]. For a single mooring breakage, the estimated losses are in the range of £2-10.5 million [4]. After considering the potential damage (safety and environmental), mandatory inspection schemes were introduced in order to monitor the structural health condition of floating platforms [3]. Standards are now in place from manufacturing through to in-situ inspection because

maintaining integrity throughout the life cycle of chains is vital. According to the DNV offshore standards [5], mooring chain links should be inspected both visually and using NDT (Non-destructive testing). Moreover, inspection of the weld seam should be carried out using ultrasonic inspection (as per ASTM E587). According to the API standards [6], material losses of 10% or more compared to the nominal as new condition must be rejected. Chain inspection intervals are determined according to the time in service. *i.e.*, a mooring system that has been in operation for 0-3 years should be inspected every 36 months, 4-10-year chain links should be inspected every 24 months and systems that are over 10 years of service should be inspected every 8 months [6].

Due to the limited access and cost of conventional inspection techniques (*i.e.* ROV inspection, chain removal, divers) in-service applications have been introduced utilising climbing and crawling robots [7], [8]. As reported in the literature, only a few attempts have been made to automate the NDT process. Compared to the overall evolution of automated NDT in industry, chain inspection is still in its infancy. Long range guided wave inspection has been used in conjunction with a climbing robot platform ''Moorinspect'' [9], [10]. A collar with guided wave transducers was fitted around a chain link using a pneumatic actuator arm, and NDT inspection was carried out. A visual inspection system was designed in 2004 to use with a climbing robot [11]. An inspection chamber was designed in this mechanism which can rotate in order to inspect orthogonal chain links. An image processing mechanism was added to the system to measure distortions of the structure. Another automated inspection system was presented in 2004, which was designed for use in the chain manufacturing process [12]. The system was designed to investigate manufacturing flaws in the weld seam by using conventional ultrasound methods. Angle probes were used in this system, and measurements were made by considering the entire curvature of the weld seam. A conceptual NDT system was proposed in 2015 by the 'chain test' project [13]. Phased array ultrasound and visual inspection were considered. A phased array system with a robotic manipulator was proposed in order to investigate the weld joint. Moreover, single degree probe ultrasonic inspection for chain crown has been studied in 2014. An NDT handle was designed to be operated by divers, but automation capabilities were not considered [14]. ROV (Remotely Operated Vehicles) are the most common industrial practice. Most ROV inspections are carried out using visual inspection *i.e.* a camera system, 3D laser surface detection mechanism [15]. Most of these visual inspection mechanisms are teleoperated and can be attached to an ROV which positions the device close to the chain. Visual inspection is based on the comparison of images, measurement readings and 3D models of the chain surface. To the best of author's knowledge very few ROV assisted examples are recorded in the literature which also include automated inspection. The system presented in [16] and [17] consists of an automated robotic manipulator which is designed to take measurements of the chain links. A gas spring measuring mechanism which is presented in [18] has been designed to record the mooring chain's physical measurements when it dragged along the chain surface by an ROV.

The current state-of-the-art automated systems are designed to only investigate the weld seam of a chain link. At TWI Cambridge, research was carried out to understand stresses between mooring chain links and potential fatigue damage. Residual stresses around the interlink contact zone were analysed during this research, and the potential fatigue damage around the crown of the chain link was investigated. Moreover, in this research, fatigue sensitivity at the 'Kt' point (approximately the region of the intrados where the shank and the crown intersect. Refer to Figure 1) was also investigated [19], [20]. During the previous automated studies, the primary concern was to investigate the weld seam of the chain. However, according to the findings in [19] and [20], chain crown inspection is also identified as crucial. Conventional NDT techniques for crown inspection are limited due to the complex geometry of the chain crown *i.e.* curved, round, overlap with the adjacent orthogonal chain link, rusted, pitted etc. To evaluate the structural health condition of a chain system, it is important to investigate the crown as well as the weld seam for possible defects such as cracks, corrosion, manufacturing defects etc. To investigate the crown and interlink contact zone, the use of both a surface penetration and amphibious method is vital. Therefore, ultrasonic inspection was selected for this study.

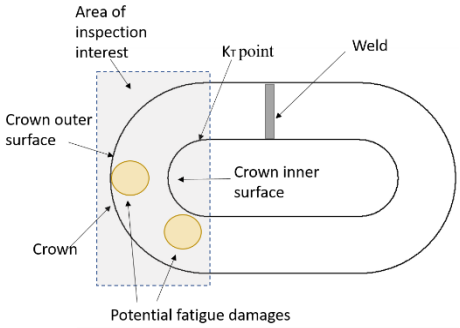


**FIGURE 1. NDT inspection focused areas due to high stress which can cause fatigue cracking [20], [19].**

This paper describes a novel application of Ultrasound Full Matrix Capture (FMC) to investigate the integrity of a mooring chain crown. The technique presented here can be adapted for use with any chain climbing mechanism, *i.e.* with robotic / automated climbing approaches. The paper is organized as follows; Section 2 reviews the background theory and modifications of the FMC algorithm. Followed by the experimental setup and a prototype. The final section presents testing and validation of the proposed system.

## II. ALGORITHM ADAPTATION FOR CURVATURE

### A. FMC BACKGROUND THEORY

FMC is an ultrasonic data collection process that uses phased-array probes to record A-Scans for every possible transmit

and receive element combination. Therefore, for a 'n' element phased-array probe, the number of A-scans is in the order of $n^2$ [21]. Prior to the technical approach of FMC, a fundamental understanding of the principle is useful. Detailed studies of the FMC have been presented in [22]–[24] and it is only briefly outlined here. The basis of the algorithm is expressed in equation (1). The FMC data acquisition along with the Total Focussing Method (TFM) was introduced to non-destructive inspection by the university of Bristol in 2005 [24] and is based on the same principles as that of synthetic aperture focussing.

$$I_{(x,z)} = \left| \sum h_{tx,rx} \left( \frac{\sqrt{(x_{tx}-x)^2+z^2} + \sqrt{(x_{rx}-x)^2+z^2}}{cl} \right) \right| \tag{1}$$

This expresses a grid of pixels that represent a cross-sectional area of the specimen of interest for inspection. The pixel intensities ($I$) is dependent on the time of flight which can be calculated using both *tx*(transmit signal) and *rx*(receive signal) *i.e.* transmit and receive. Where $h$ is the Hilbert transform which allows for the complex signal to be extracted from time domain data. This is useful in determining the signal magnitude (envelope). By calculating the complex signal, this can create the signal magnitude envelope. Each pixel intensity in the image, *I(x,z)*, is determined by equation (1). Previous work presented [22] showed how the parallel processing capabilities of modern graphics cards could be utilised to accelerate the processing of the algorithm. Modification of the basic FMC equation (1) has been studied [25] to focus the sound beam through dual media *i.e.* when the probe is placed in water and inspection is carried out inside a metal. Equation (2) has been developed according the dual media refraction. Where the intensity value of the pixel locating *x, z* is $I$, which has been determined by each *tx* and *rx* pair to the pixel region of interest (*x, z*). via the point at which the ultrasonic energy passes through the refractive interface ($x_{txi}$, $z_{txi}$ for transmit and $x_{rxi}$, $z_{rxi}$ for receive) to the pixel location. The velocity in the medium is $c$ and the velocity though the interface material is $cl$.

$$I_{(x,z)} = \left| \sum h_{tx,rx} \times \left( \frac{\sqrt{(x_{tx}-x_{txi})^2+z_{txi}^2} + \sqrt{(x_{rx}-x_{rxi})^2+z_{rxi}^2}}{cl} + \frac{\sqrt{(x_{txi}-x)^2+(z-z_{txi})^2} + \sqrt{(x_{rxi}-x)^2+(z-z_{rxi})^2}}{c} \right) \right| \tag{2}$$

### *B. SURFACE MAPPING*

#### 1) SURFACE MAPPING REQUIREMENT

For inspections which are carried out with a static wedge, the ultrasonic transmission paths can be computed once before any signal processing commences. However, for chain inspection the probe is separated from a curved surface of unknown geometry (*i.e.* curved geometry of the chain after wear) by a water path of around 35-40mm, *i.e.* requirement of the water path and the height is discussed later (section III). which presents additional problems: 1. the surface must be mapped and then 2. ultrasonic transmission paths must be recalculated based on this surface. Therefore, the adaptations which are mentioned below has been added to the existing algorithm. Three algorithms for surface mapping were evaluated in order to determine the most optimum for the geometry considered here. *i.e.* mooring chain's curved surface. The front wall is typically of little interest, so it is usual for responses from this region allowed to be saturated in favour of acquiring good signals in the region of interest (from inside the material). Conversely, when surface mapping the ultrasonic signal from the front wall is of critical interest and a saturated front wall signal will lead to inaccuracies in the estimation of the front wall position. For this reason, the imaging algorithm at each transducer position was sub-divided into two acquisitions, (a) Surface mapping acquisition performed at lower gain, so as not to saturate the front wall response. (b) An imaging acquisition with a higher gain in order to maximise the signal-to-noise ratio of the FMC data set.

#### 2) VERTICAL PROJECTION

In this algorithm, each element is fired separately in pulse-echo mode, and the distance to the front wall is derived from the water velocity and the time to the first response. A typical front wall response is illustrated in Figure 2(a). As the location of each transducer is known, the surface can be constructed by positioning the surface point directly below it. An example plot of this algorithm is shown in Figure 2 (b).

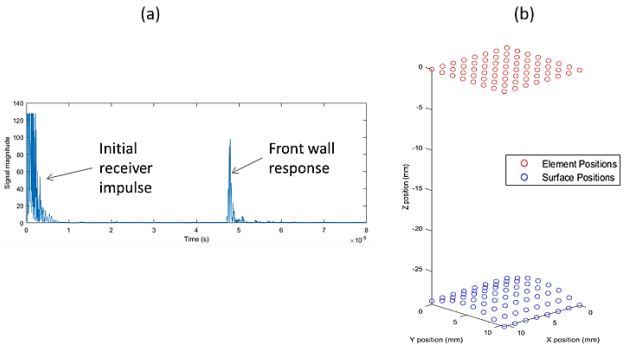


**FIGURE 2. (a) Sample ultrasonic response that has the initial receiver impulse and the front wall response (reduced gain). (b) Example output of the vertical project algorithm showing transducer positions (red) and surface positions (blue).**

#### 3) DIPPING REFLECTORS

Studies conducted in [26] show that unless the surface is flat and parallel to the plane in which the transducer elements are in contact, vertical projection mis-plots the position of the surface. However, if the surface can be assumed to be flat

between adjacent pairs of transducer elements then the dipping reflector algorithm can be used. Each transducer emits a spherically spreading wave that bounces of the front wall and returns to the element. The signal paths are orthogonal to the front wall in each case therefore the angle of incidence and angle of reflection must be equal. Differences between lengths of two paths are used to calculate the shifts in the horizontal ($\Delta x$) and vertical ($\Delta z$) directions, where s is the element pitch (refer to Figure 3(a), equation (3) and (4))

$$\Delta x = \Delta z \frac{(d_2 - d_1)}{s} \tag{3}$$

$$\Delta z = \frac{d_2}{\sqrt{1 + \frac{(d_2 - d_1)^2}{s^2}}} \tag{4}$$

On a three-dimensional surface, groups of four neighbouring elements are considered where the front wall is assumed to be planar between responses from each group of four. An average gradient is computed in the passive and active directions of the probe as shown in Figure 3(b) & (c). The final position of the point on the surface generating the signal for each element can then be calculated as a combination of two shifts, a vertical shift parallel to the z axis, and a shift in the x-y plane.

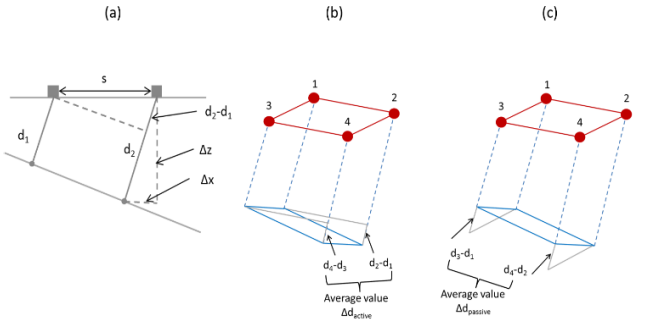


**FIGURE 3.** (a) Calculation of the shift in x and z from the transducer location using the difference in paths d1 and d2. (b) and (c) Calculation of the average gradient in the active x and passive y array (blue).

#### 4) POINT LIKE REFLECTORS

The point-like reflector algorithm assumes that the response received by two adjacent transducer elements originated from the same point on the surface. For linear phased-array probes a detailed methodology of this algorithm is given in [27]. Adapting this algorithm for 2D probes involves locating the intersection point of three neighbouring transducers. Graphically, the fundamental principle of this technique is presented in Figure 4. The x, y and z location of the intersection point of these three spheres relative to the centre of sphere 1 are given by Equation (5), (6) and (7).

$$y = \frac{r_1^2 - r_3^2 + j^2 + i^2}{2j} - \frac{i}{j}x \tag{5}$$

$$\mathrm{x} = \frac{r_1^2 - r_2^2 + d^2}{2d} \tag{6}$$

$$\mathrm{z} = \pm\sqrt{r_1^2 - x^2 - y^2} \tag{7}$$

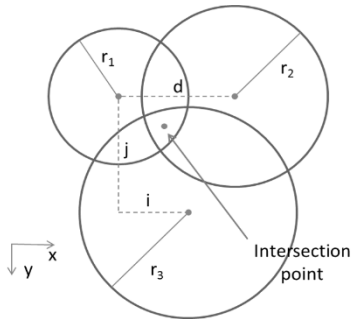


**FIGURE 4.** Calculation of the inspection point of three spheres array directions.

## III. DESIGN APPROACH

### A. FRONT WALL MAPPING; SELECTION TEST

After considering the above surface mapping methods, a laboratory experiment was carried out in order to select a suitable method for chain inspection. An experiment was set up as illustrated in Figure 5 and the responses from focusing techniques were analysed. Selecting a suitable mapping technique was the primary concern of the following experiment. A 3D printed probe holder which is illustrated in the Figure 5(a) was constructed to place the probe on the chain surface. The holder was capable of changing the probe's angle and chain-probe height. Permanent magnetic adhesion attachments were proposed to keep the probe steady on the chain surface. The probe was placed on the chain surface as illustrated in Figure 5(b) with the aid of magnetic adhesion. Then the air gap between the probe and the chain surface was filled with water (refer to Figure 5(c)). The gap between the probe and the chain surface (water path) was calculated as ≈40mm in order to avoid front wall reflections when the maximum inspection depth is ≈134mm. A water path was introduced as a couplant to replicate the mooring chain in-situ conditions, i.e. subsea condition. Continuous water supply has been used previously during NDT automation in [28] and [29]. After the experimental setup, comparisons between the vertical projection, dipping reflectors and the point-like reflector algorithms were studied. The results are shown in Figure 6, Figure 7, Figure 8 respectively. The experiment was carried under static water conditions.

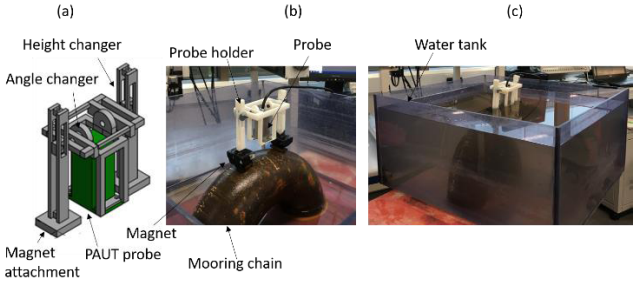


**FIGURE 5.** (a) CAD model of the Probe holder. (b) Experimental setup. (c) Full experimental setup; submerged condition.

The point-like reflectors algorithm did not produce a satisfactorily accurate surface map (refer to Figure 8).

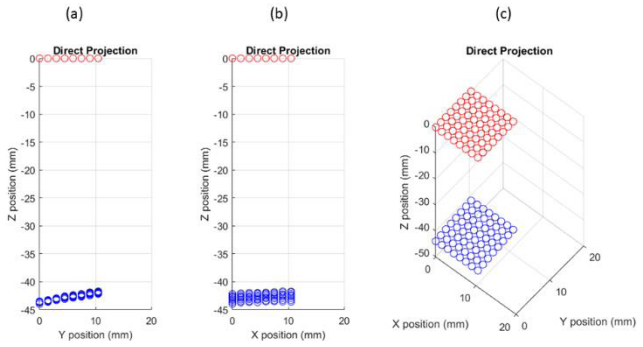


**FIGURE 6.** Example surface mapping results for the direct projection algorithm (a) y -z mapping. (b) x – z mapping. (c) x-y-z surface mapping sample.

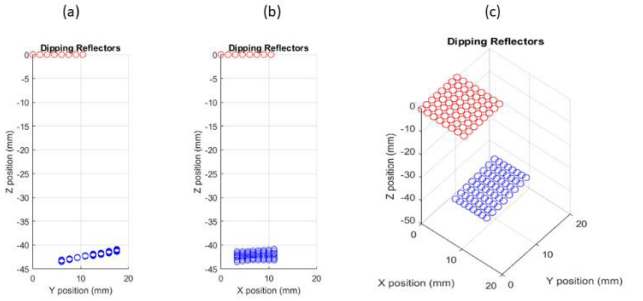


**FIGURE 7.** Example surface mapping results for the dipping reflectors projection algorithm (a) y -z mapping. (b) x – z mapping. (c) x-y-z surface mapping sample.

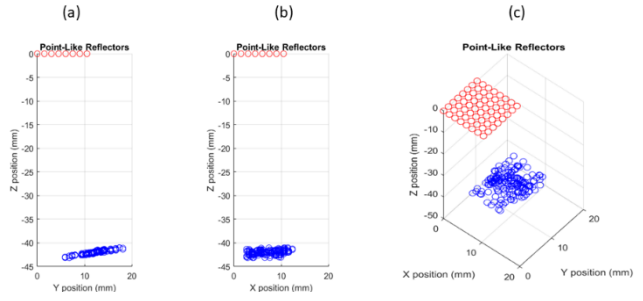


**FIGURE 8.** Example surface mapping results for the point like reflectors projection algorithm (a) y -z mapping. (b) x – z mapping. (c) x-y-z surface mapping sample.

According to the illustrated results, computed surface points would be a long way (>20mm) from their expected approximate position. Instabilities in the temporal domain were also observed. Given that this test was performed in laboratory conditions with stationary sample and probe, this algorithm was deemed unsuitable for surface mapping in this application. In contrast, the dipping reflectors algorithm exhibited better performance in terms of mapping the curvature of the sample map (refer to Figure 7). It was still slightly unstable in the temporal domain. Potential improvements to the algorithm could be implemented to provide a number of ultrasonic acquisitions to average out some of the noise. Given that acquisition time is important for this application, this avenue was not pursued. The vertical projection algorithm proved to be very stable during the experiments (refer to Figure 6). Given that these were performed in ideal conditions, and that conditions in the field are likely to be more challenging, the vertical projection algorithm was chosen as the surface mapping technique.

### B. WEDGE DESIGN

As mentioned previously, the intention of this research is to check the feasibility of using phased array ultrasound-based FMC to inspect the chain crown region in both air and under water. In air, ultrasound inspection is a challenging task compared to underwater. *i.e.* an additional coupling medium is not required for underwater ultrasound inspection. When considering in air inspection, using water as a couplant for automated NDT is a common industrial approach. Most of the 'in air industrial applications' that use water as a couplant conduct inspection in pipes, tubes, plates etc. (hollow tube-like or thin structures). Due to the significant curvature of the mooring chain (*i.e.* ≈66.5mm radius) and the large thickness (*i.e.* outer surface to the inner surface ≈133mm) a custom-built water coupling mechanism was required with the following specifications, 1. It should be capable of being placed on the chain surface, 2. The wedge should be able to provide a sufficient water path between the chain surface and probe (*i.e.* 40mm), 3. The wedge should be used as an attachment during the automation process, 4. The wedge should always place the probe face perpendicular to the chain surface. As discussed earlier, phased array is a common NDT tool for robotics and automation *i.e.* phased array is capable of covering an area under the probe due to its beam steering capability. Minimising the number of probe placement points on the chain surface was considered as an advantage because having a discreet inspection will ease the automation process *i.e.* if a continuous reading is required, the probe must be travelled along the chain surface, and discreet inspection is similar to a spot scan. Therefore, a submergible 2D phased array probe with the specifications in Table 1 was selected.

**TABLE 1.** Phased array probe specifications.

| Characteristics / Parameter | Value / acceptance criteria |
|---|---|
| Centre frequency (-6dB) | 5±0.5 MHz |
| Bandwidth (-6dB) | ≥60% |
| Pulse length (-20dB) | ≤ 0.8µs |
| Sensitivity homogeneity | ± 3dB |
| Geometrical shape | 2-D array |
| Number of channels | 64 |
| Elementary pitch | 1.5mm |
| Elements interspace | 0.1mm |
| Elevation | 1.5mm |

A specification study was carried out to determine the physical parameters of the wedge. Unlike pipeline inspection, the thickness of mooring chains is significantly greater

(∼133 - 134mm in this study). It was necessary to understand the required length of the water path in order to reduce/avoid front wall reflection (40mm water path). As was explained previously, cracks are commonly found in the interlink contact zone of the chain link (refer Figure 1), therefore, 100-134mm thickness range was selected for inspection (refer Figure 9). This study aims to automate in air NDT inspection of mooring chains by using a robotic arm (the design of the robotic manipulator is discussed later). Therefore, a wedge attachment with the end effector of the robotic manipulator was developed during the design phase. Figure 10 (a) illustrates the main components of the probe holder/continuous water supply wedge. *i.e.* a-NDT probe, b-water inlet 1, c-water inlet 2, d-spring, e-excess water outlet, f-robotic manipulator mount, g-curved edge, h-wedge tightening (clamping) screw holes, carbon fibre wedge holding bars, j-locking nut, k-spring guiding bars. The wedge was designed to maintain the water path during the inspection. Water bubbles in the water pocket were found to disrupt the sound path, therefore, two continuous water supplies were added to the design with an overflow outlet to ensure water bubbles are flushed out as illustrated in Figure 10. Due to the rough and robust surface nature of mooring chains, a marine grade silicon layer was proposed for the contact surface of the wedge (as the wedge-chain contact layer). Compression of the silicon gasket against the chain was used to minimise the water leakage (water leakage from chain-wedge contact surface). The curved face of the wedge was introduced to reduce the required thickness of the gasket and increase the adaptability to the chain curvature. Moreover, the curvature of the wedge was designed according to the chain's surface curvature (refer Figure 10(d)). Using an automated manipulator for chain inspection is one of the main purposes of this study. A passive compliant mechanism (spring mechanism) was added between the robotic manipulator mount and end of the wedge. The force created by the compression of springs allows the silicon gasket to settle on the chain surface and the passive compliance corrects the small nominal deviation of the wedge *i.e.* at a given point, it is essential to maintain the position of the probe normal to the inspection surface.

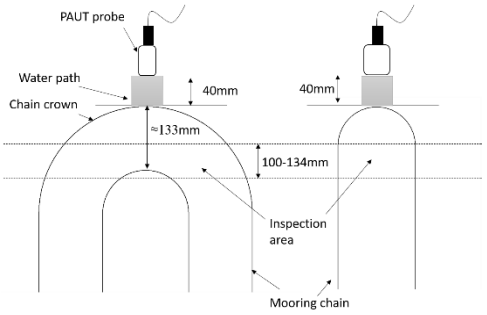


**FIGURE 9.** NDT probe holder/ wedge design requirements.

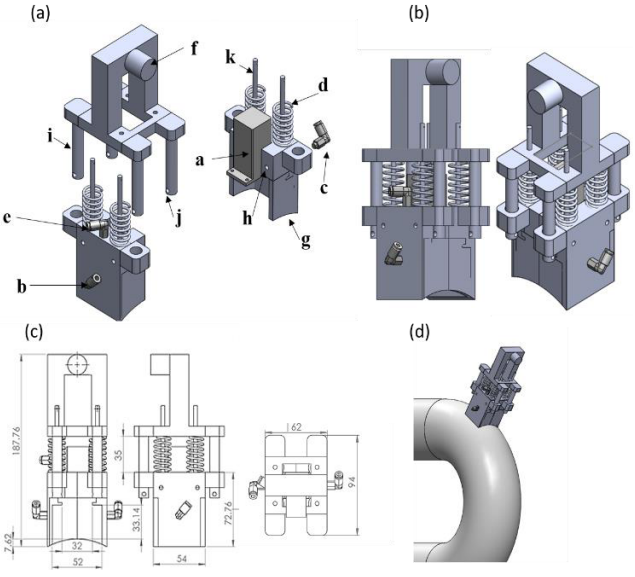


**FIGURE 10.** (a) Exploded view of the wedge design. (b) 3D- CAD model. (c) 2D schematics. (d) Probe holder placement on the chain surface.

### C. AUTOMATED MANIPULATOR REQUIREMENTS

A feasibility study to use phased array with a robotic arm to obtain NDT results (in the chain crown area) was the primary concern of this study. As was mentioned previously, a number of discrete inspection points along the chain surface were selected for the phased array inspection. The pre-planned placement of the probe has to be programmed in order to conduct a full crown inspection. *i.e.* in the form of a raster scan along the chain crown. When considering the ultrasound probe locations (on a mooring chain crown) explained in [14], a raster scan along the chain crown is needed to improve the investigation (as illustrated in the Figure 11). The gap between any two scan points was determined according to the scanning requirement *i.e.* a close gap between two spot scans leads to a better result. Scanning across the chain surface is limited due to the adjacent orthogonal chain link. A single

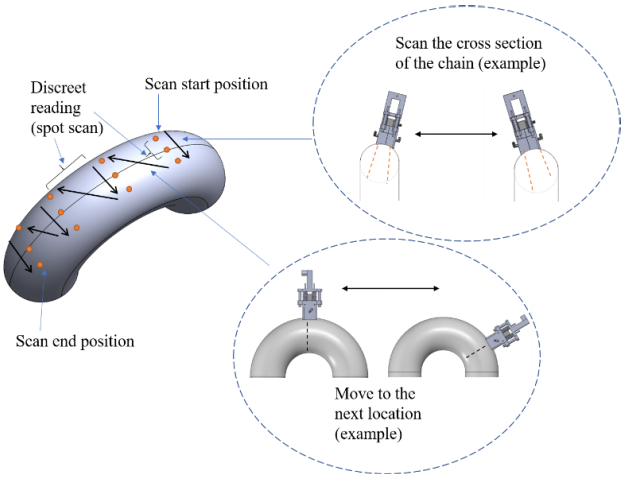


**FIGURE 11.** Proposed mooring chain scanning steps (for an automated manipulator).

chain piece was used in this experiment, but an adjacent chain link is always present for in-situ chain environments.

A robot manipulator design was carried out according to the wedge positioning requirements. When considering the wedge orientations (refer to Figure 12), 5 DoFs can be observed to scan the cross-section, *i.e.* translations around z, y-axes and rotation around the x-axis (refer to Figure 12(a)). For a scan along the crown of the chain, translations in x, y-axis and rotation along the z-axis are needed as illustrated in Figure 12(b). In summary, three translations (along x, y & z) and two rotations (around x and z) are needed for chain crown raster investigation. When considering the geometrical features of the manipulator requirements, x, y, z translations can be modelled with a Cartesian (gantry type ) manipulator that has a two-axis wrist which carries the tool frame (wedge). After considering the requirements, a robotic manipulator which is illustrated in Figure 13 is proposed, where L1-L8 are mechanical attachment clearances, d1, d2, d3 are the linear axis variables in z, x, y directions respectively and Ø1, Ø2 are rotary axes variables in z, x-axes respectively.

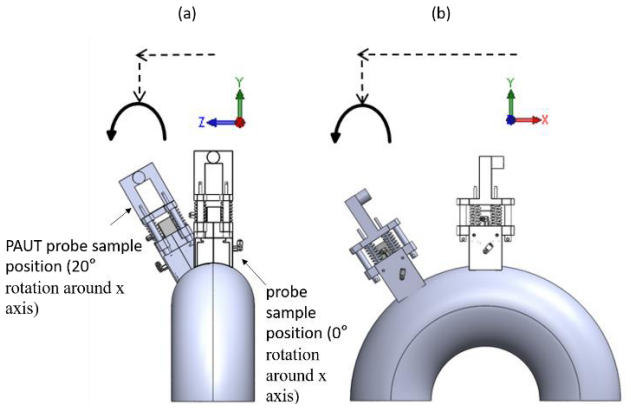


**FIGURE 12.** **(a) Chain cross section scan requirements. (b)Chain scan long the crown requirements.**

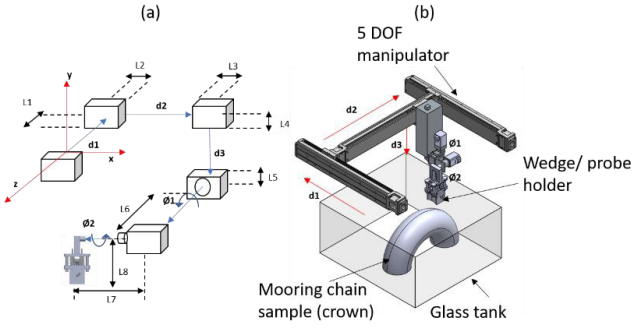


**FIGURE 13.** **(a) Schematics of the proposed manipulator. (b) CAD model of the proposed manipulator.**

## IV. EXPERIMENTAL SETUP AND PROTOTYPE

It was necessary to select an appropriate set of springs to provide suitable compression force (the springs are illustrated in Figure 10(a)). Therefore, a simple experiment was carried out as illustrated in Figure 14. A mooring chain sample was

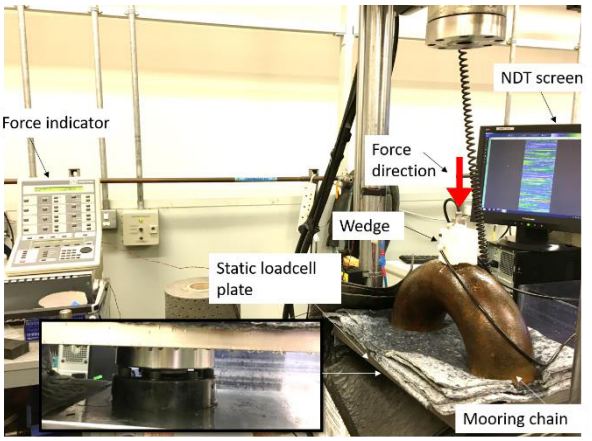


**FIGURE 14.** **Spring force requirement test rig.**

placed on material testing equipment with a static loadcell. Then a perpendicular force was applied to the wedge (sample wedge without the manipulator attachment) as illustrated by the red arrow in Figure 14 (*i.e.* incremental force was applied to the wedge). Once the NDT results were satisfactory, the corresponding force was recorded. The experiment was repeated ten times, and the average readings were considered (10 readings for each position). The wedge was moved along the chain surface and readings were taken. According to the experimental results, 8N to 13N force needs to be applied by springs. This applied force deforms the silicon gasket to make the wedge on the chain surface watertight. Four compression springs ( 0.72N/mm each) were added to the system to provide the required force. A 13N force was obtained by compressing each spring by ≈4.6mm.

To test the proposed 'continuous water supply wedge', a model was rapid prototyped as illustrated in Figure 15. In order to mount the PAUT (phased array ultrasonic) probe, the water pocket area of the wedge was split into two main parts as illustrated in Figure 15(a). The pocket was assembled and tightened after placing the probe on the holding edges.

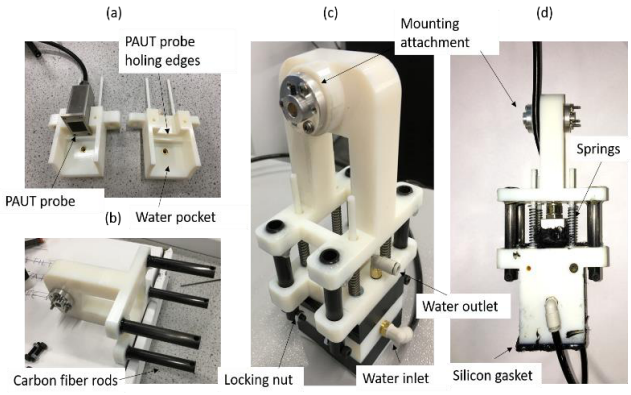


**FIGURE 15.** **Prototype of the continuous water supply wedge. (a) Water pocket and the PAUT probe. (b) Manipulator attachment. (c)&(d).**

The manipulator attachment was built as a separate module (refer Figure 15(b)) and then inserted into the wedge with the use of carbon fibre rods and locking nuts as illustrated in Figure 15(c). Finally, springs and the silicon gasket which are illustrated in Figure 15(d) were added to the system.

The automated manipulator proposed in Figure 13 was prototyped and the wedge was attached as illustrated in Figure 16. The x, y, z linear axes were driven with linear slide actuators (lead screw model, refer Figure 16(d)), and each axis was actuated by a DC 24V stepper motor. Hard rubber stoppers and magnetic limit switches were added to the linear axes to prevent slider collisions during experiments.

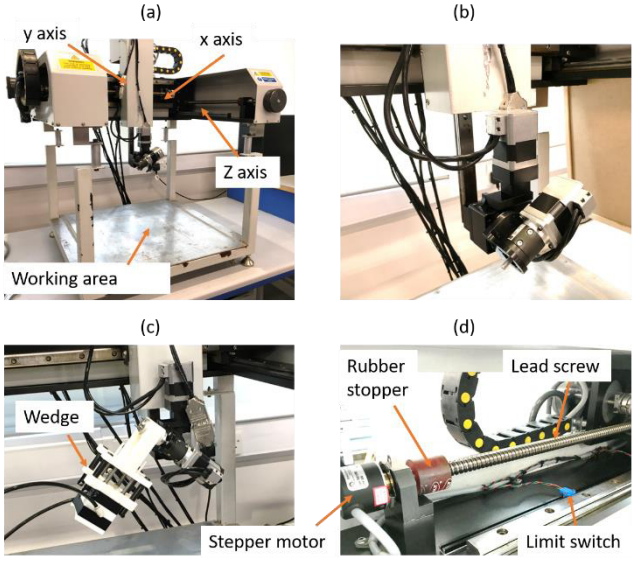


**FIGURE 16.** **Automated 5DOF manipulator. (a) 5axis manipulator test rig. (b) 2 rotary axis closer view. (c) Wedge attachment. (d) Axis components.**

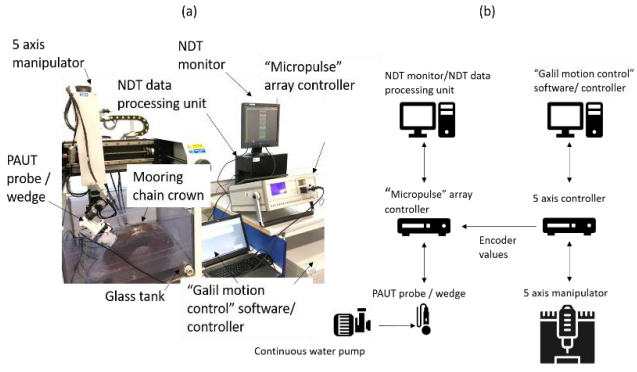


**FIGURE 17.** **(a) Physical experimental setup. (b) Experimental setup block diagram components.**

The experimental setup which is illustrated in the Figure 17(a) was created according to the block diagram illustrated in Figure 17(b). As discussed previously (refer to Figure 10 (a)), two water inputs were added to the wedge during the prototyping stage. Therefore, two IP 68 12V DC water pumps (rated at 300 l/h each) were attached to the wedge with the use of pneumatic push-fit connections. A five axis controller was programmed using ''Galil Tools'' software control language [30] and connected to other components with an ethernet connection. Similarly, the PAUT array was controlled by a ''Micropulse'' array controller [31] and relevant commands were generated on a sperate processing unit (TWI PAUT processing unit/software CRYSTAL$^{TM}$ [32]). During this experiment, control of the NDT system and the manipulator system was carried out separately *i.e.* no feedback data/signals were exchanged between systems.

As illustrated by Figure 17(b), Galil Tools motion control software was used to program the inspection path which was described in Figure 11. In order to execute the inspection, the tool frame (PAUT probe and the wedge) was moved along the chain surface, and the encoder readings of 5 axes were recorded. Distances/angles for two example inspection points are illustrated in the Figure 18. Figure 18(a)-(b) illustrates axis variations during two inspection points along the chain, and Figure 18(c)-(d) shows the axis variation during the cross-section inspection. In Figure 18, the A, C, B axis represent a x, y, z Cartesian axis system (in Figure 13) respectively. Rotation along the x-axis is represented by 'D' axis and rotation around z is represented by the 'E' axis. Moreover, each inspection point was represented by five encoder values (three distances, two angles) and the values were stored in the control software in order to execute the inspection path. As was mentioned previously, having air bubbles in the water chamber prevents good inspection results. Therefore, a 15s delay was introduced before reading the data from the NDT display.

A chain crown with a diameter of ≈133mm was used in this experiment. Four defects (drilled hole/flat bottom type) were introduced to the inner surface of the chain as illustrated in Figure 19. Defect 1, 3 were placed perpendicular, and 2,4 were placed 20 degrees from the perpendicular position as illustrated in Figure 19(b). Defects with ≈5mm diameter were introduced. The defect lengths are discussed in the results section.

## V. RESULTS AND DISCUSSION

The phased array inspection was carried on the outer surface of the crown by placing the continuous water supply wedge with the automated manipulator. The Phased Array FMC results were displayed with the use of the TWI CRYSTAL$^{TM}$ software [32]. The raster scan which was proposed in Figure 11 was carried out with the automated 5 DoF manipulator as illustrated in Figure 20. Figure 20(a) illustrates inspection examples of cross-section inspection and Figure 20(b) illustrates along the chain crown inspections.

According to the mooring chain inspection standards, it is crucial to check the material loss in the chain interlink contact zone. Therefore, back wall thickness was investigated as illustrated in Figure 21 (a) ('no defect' reading). FMC images of defects (refer Figure 19) are illustrated in Figure 21 (b) - (e) where the back wall of the chain (inner crown surface) and the defect height is presented. With the proposed NDT

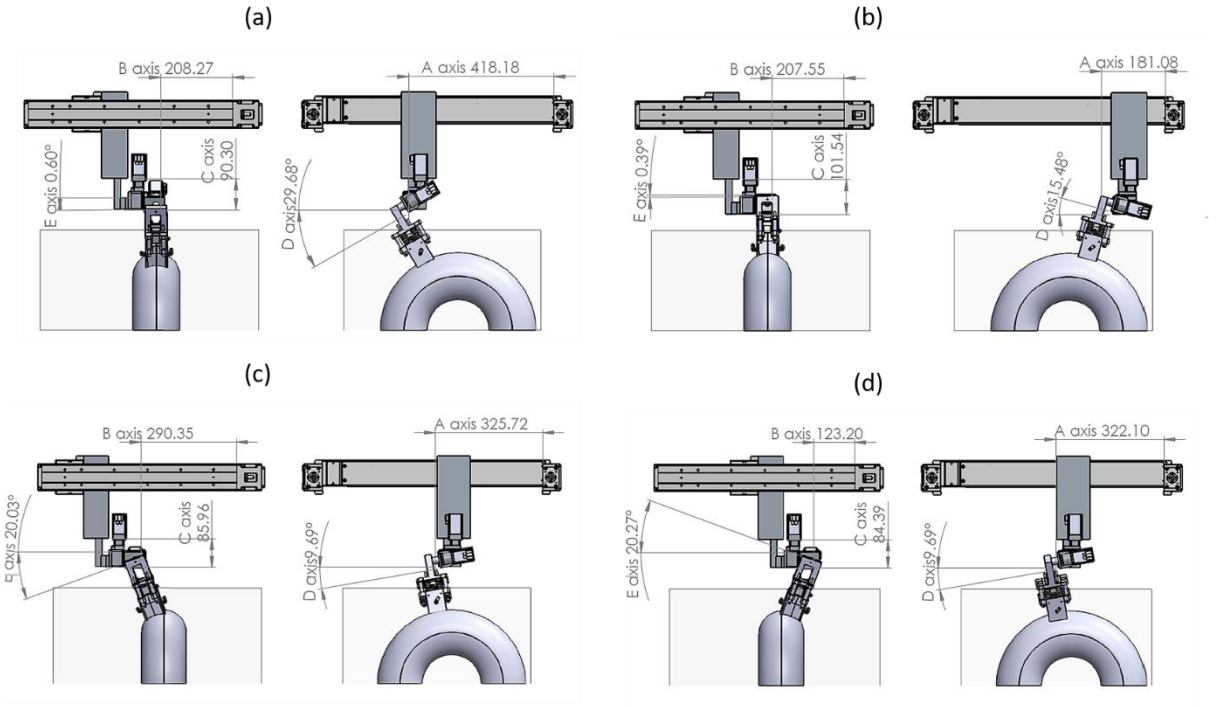


**FIGURE 18.** Inspection points examples. (a) Inspection along the chain crown point example point 1. (b) Inspection along the chain crown point example point 2. (c) Inspection across the chain cross-section example 1. (d) Inspection across the chain cross-section example 2.

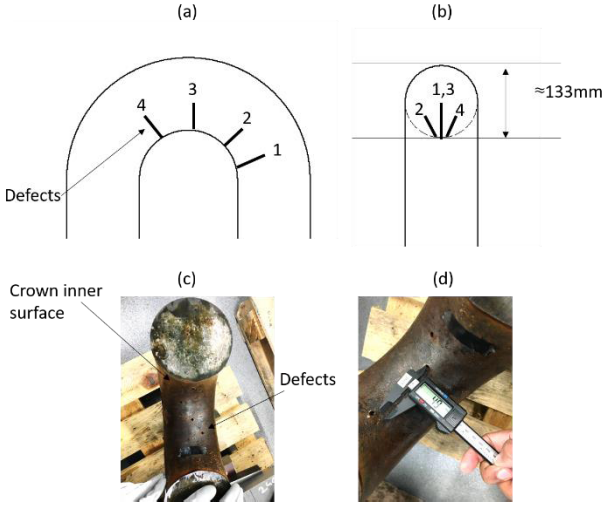


**FIGURE 19.** (a) Drilled hole defects in chain crown (side view). (b) Drilled hole defects in chain crown (cross-sectional view). (c) Defects image. (d) Defect hole diameter (sample).

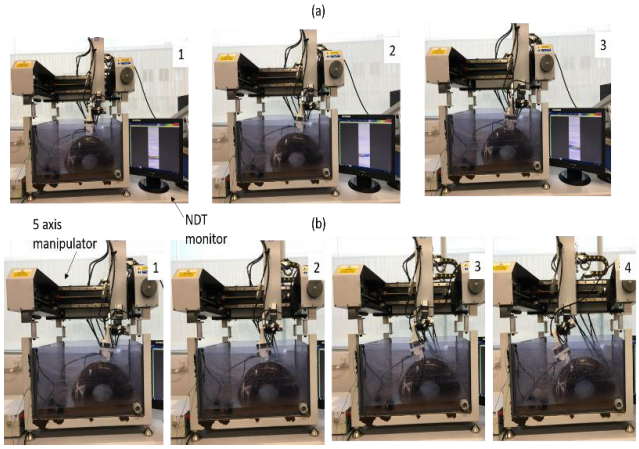


**FIGURE 20.** (a) Inspection example – cross section of the chain. (b) Inspection example – across the chain crown surface.

imaging technique, depth of the defect can be measured. The distances between the top of the defect and the back wall are shown in the images. The results presented in Figure 21 were recorded during in-air inspection, and defect depth results were compared (refer to Table 2) with underwater inspection results (taken without the wedge) and measured depth values (mechanical measurement using a calliper). The experiment was repeated five times, and the average readings were calculated (5 readings for each position).

According to the comparison which is illustrated in the Table 2, it is significant that the proposed technique is capable

**TABLE 2.** NDT results comparison.

| Defect No | In air UT results / SD | Underwater UT results/ SD | Measured Depth of the defect |
|---|---|---|---|
| 1 | 15.28mm /0.14 | 16.14mm/0.10 | 15.50mm |
| 2 | 11.39mm/0.24 | 11.93mm/0.16 | 12.00mm |
| 3 | 11.25mm/0.17 | 11.39mm/0.29 | 11.00mm |
| 4 | 16.45mm/0.10 | 15.68mm/0.02 | 16.00mm |

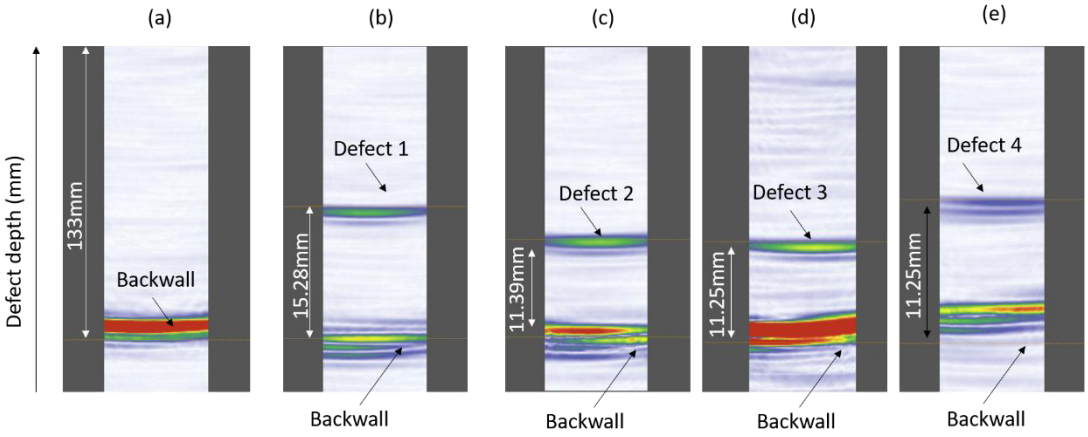


**FIGURE 21.** Experimental results. (a) Sample back wall ( no defect). (b) Defect 1 scan results. (c) Defect 2 scan results. (d) Defect 3 scan results. (e) Defect 4 scan results. (f) Defect 5 scan results.

of identifying defects (as illustrated in Figure 19 and results illustrated in Figure 21 are similar). The defect sizing was not part of this study. However, defect depth (height between the top of the defect and back wall of the chain) was measured with the present technique. In air results (with the use of continuous water supply wedge) and directly measured depth results (mechanical measurement) are in good agreement, with the maximum variation being 0.61mm (≈5% discrepancy). When comparing in water results and the mechanical depth reading of the defect, it is possible to conclude that the proposed technique is able to successfully operate in both air and underwater. Due to the amphibious nature of the mooring chains, it is essential to develop a technique that can be automated as well as capable of operating both in the air and underwater. Moreover, the proposed technique can be used to evaluate material losses in the chain by measuring the thickness of the chain diameter as illustrated in Figure 21(a). If there is material loss, the back-wall reading is less than the nominal (expected) value. With the development of amphibious mooring chain climbing robots (*i.e.* [7], [8], [10], [33]) automated comprehensive integrity management techniques can be taken to the chain in service. Therefore, automated capability of the technique is essential. According to the experimental results (Figure 20-21 and Table 2), the proposed amphibious technique can be automated and adapted for integration with a climbing robot.

## VI. CONCLUSION AND FURTHER WORK

While ultrasound inspection of the chain weld area is mandatory and it is standard practice, recent investigations have identified the chain crown as a crucial area for inspection. At present, in service ultrasound inspection of the chain crown is not a state of the art inspection procedure due to the operational difficulty. However, with the development of robotic/automated climbing mechanisms, conventional NDT techniques *i.e.* ultrasonic testing, can be used to assess the structural health of mooring chains. Ultrasound inspection was selected for chain crown inspection due to its ability to penetrate large chain link thickness, the amphibious nature of the inspection task and automation capability. Phased array ultrasound was considered in order to ease the automation by using its discreet inspection capability. Mooring chain integrity assessment with the phased array is still in its infancy due to the infield operational complexities and the geometrical features of the chain. An amphibious automated NDT technique is proposed in this feasibility study which can be used to assess the structural health of mooring chains. The FMC data acquisition technique was used in the interest of enhancing the quality of the NDT images. The FMC technique was adapted according to the mooring chain's curved surface. In order to adapt, three surface mapping techniques were evaluated during this research, and a suitable technique was selected. Mooring integrity inspection has to be conducted in both air and underwater. Therefore, a continuous water supply wedge was designed to provide a marine coupling environment in air. A 5-axis automated manipulator was designed to simulate the automated inspection capability.

The proposed phased array automated inspection system was tested with simulated defects *i.e.* drilled hole type defects. Within this study, a novel application of FMC /phased array was demonstrated for chain crown inspection, and laboratory experiments were carried out with use of an automated manipulator. According to the results obtained, it is possible to state that the proposed automation friendly technique is suitable for chain crown ultrasound inspection.

Further work should be carried out in order to develop a fully functional industrial chain inspection system. At the moment, defects are displayed but a comprehensive defect identification algorithm (*i.e.* crack, corrosion, hole, etc.) needs to be implemented. Phased array controller and the NDT system were used in laboratory conditions where size and weight did not matter. However, for field work the physical size should be minimised for integration with a climbing robot. The robotic manipulator which was prototyped in the research was designed for laboratory-based experiments (*i.e.* heavy stand, not suitable for in-situ mooring conditions). For subsea applications, it will need to be marinized, ruggedized and miniaturised in order to mount on a climbing robot.

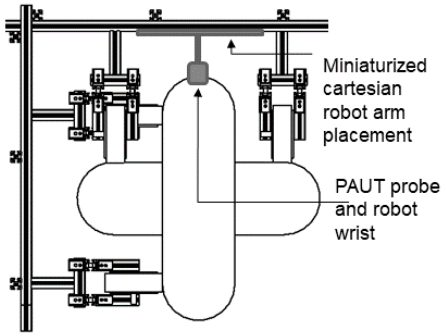


**FIGURE 22.** **Proposed miniaturized robotic manipulator attachment.**

An example (proposed for future development) of robot attachment is illustrated in Figure 22. The chain geometry was known in this research but in real applications the geometry may differ. Therefore, an automated chain crown shape detection mechanism will be required. The experiments were carried out to perform NDT of the crown but the proposed technique can be evolved to investigate both the crown and the weld at the same time with a single system.

## ACKNOWLEDGEMENT

The authors express their sincere gratitude to the staff of LSBIC, TWI (NDT - Cambridge / TWI Technology Centre - Wales), Dr Philippe Bastide, Dr Channa Nageswaran, Ivan Pinson, InnotecUK and Brunel Innovation Centre, Cambridge for their support.

## REFERENCES

[1] P. Elman, J. Bramande, E. Elletson, and K. Pinheiro, "Reducing uncertainty through the use of mooring line monitoring," in *Proc. Offshore Technol. Conf.*, Rio de Janeiro, Brazil, 2013.

[2] K.-T. Ma, H. Shu, P. Smedley, and A. Duggal, "A historical review on integrity issues of permanent mooring systems," in *Proc. Offshore Technol. Conf.*, Houston, TX, USA, 2013.

[3] Á. Angulo, G. Edwards, S. Soua, and T.-H. Gan, "Mooring integrity management: Novel approaches towards *in situ* monitoring," in *Structural Health Monitoring—Measurement Methods and Practical Applications*. Rijeka, Croatia: InTech, 2017, pp. 87–108.

[4] *Floating Production System—JIP FPS Mooring Integrity*, Noble Denton Europe Limited, Health Safety Executive, Bootle, U.K., 2016.

[5] *DNV-OS-E303. Offshore Mooring Chain*, DNV, Oslo, Norway, 2013.

[6] *In-Service Inspection of Mooring Hardware for Floating Structures*, Amer. Pertroleum Inst., Washington, DC, USA, 2008.

[7] M. Dissanayake, T. P. Sattar, O. Howlader, I. Pinson, and T.-H. Gan, "Tracked-wheel crawler robot for vertically aligned mooring chain climbing design," in *Proc. IEEE Int. Conf. Ind. Inf. Syst. (ICIIS)*, Peradeniya, Sri Lanka, Dec. 2017, pp. 1–6.

[8] M. Dissanayake, T. Sattar, T.-H. Gan, I. Pinson, and S. Lowe, "Design and prototype of a magnetic adhesion tracked-wheel robotic platform for mooring chain inspection," *Proc. Inst. Mech. Eng. I, J. Syst. Control Eng.*, vol. 232, no. 8, pp. 1063–1074, 2018.

[9] A. G. Ruiz, T. P. Sattar, C. M. Sanz, and B. S. Rodriguez-Filloy, "Inspection of floating platform mooring chains with a climbing robot," in *Proc. 17th Int. Conf. Climbing Walking Robots Support Technol. Mobile Machines*, Poznań, Poland, 2014, pp. 251–258.

[10] G. R. Edwards, S. Kokkorikos, A. Garcia, C. Patton, and T. Sattar. *Moorinspect*. Accessed: Aug. 6, 2018 [Online]. Available: http://www.bindt.org/downloads/ndt2012_3c1.pdf

[11] P. Weiss, F. Andritsos, F. Schom, and A. Fidani, "Innovative robotic solutions for the survey and certification of ships and mobile offshore units," in *Proc. COMPIT*, Sigüenza, Spain, 2004, pp. 1–8.

[12] J. L. García, E. García, C. M. Suárez, D. Blanco, and N. Beltrán, "Automated Off-shore studless chain inspection system," in *Proc. 16th WCNDT - World Conf. NDT*, Montreal, QC, Canada, 2004.

[13] S. Williams. *Autonomous Robotic System for the Inspection of Mooring Chains that Tether Offshore Oil and Gas Structures to the Ocean Floor*. Accessed: Nov. 26, 2018. [Online]. Available: https://cordis.europa.eu/result/rcn/46870_en.html

[14] J. Rudlin, "Multi-channel ultrasonic inspection of a mooring chain for fatigue cracks," in *Proc. Eur. Conf. Non-Destructive Test.*, Prague, Czech Republic, 2014.

[15] Savante Offshore Services Ltd. (2017). *Subsea-Laser-Mooring-Chain-Scans*. Accessed: Aug. 6, 2018. [Online]. Available: https://www.savante.co.uk/subsea-laser-mooring-chain-scans/

[16] A. D. Hall and G. M. Lethbridge, "Digital imaging for subsea operations: Innovative ROV tooling and image analysis combinations for mooring chain assessments yield cost savings and operational confidence for offshore operators," in *Proc. Offshore Eur. Oil Gas Exhib. Conf.*, Aberdeen, U.K., 1999.

[17] (2017). *Welapetage*. Accessed: Jun. 25, 2018. [Online]. Available: http://www.welaptega.com/ and http://www.welaptega.com/services/subseameasurement/

[18] M. Yoshie and T. Tanaka, "Field test of a practical test model of maintenance examination system for mooring facilities and additional installation of chain grasping frame in the vehicle," in *Proc. IEEE Int. Underwater Technol. Symp. (UT)*, Tokyo, Japan, Mar. 2013, pp. 1–8.

[19] P. Bastid and S. D. Smith, "Numerical analysis of contact stresses between mooring chain links and potential consequences for fatigue damage," in *Proc. ASME 32nd Int. Conf. Ocean, Offshore Arctic Eng.*, Nantes, France, 2013.

[20] I. M. Perez, P. Bastid, and V. Venugopal, "Prediction of residual stresses in mooring chains and its impact on fatigue life," in *Proc. ASME 36th Int. Conf. Ocean, Offshore Arctic Eng.*, 2017, p. V03AT02A034.

[21] R. D. Tech, *Introduction to Phased Array Ultrasonic Technology Applications: R/D Tech Guideline*. Canada: R.D Tech Inc., 2004.

[22] M. Sutcliffe, M. Weston, B. Dutton, P. Charlton, and K. Donne, "Real-time full matrix capture for ultrasonic non-destructive testing with acceleration of post-processing through graphic hardware," *NDT E Int.*, vol. 51, pp. 16–23, Oct. 2012.

[23] C. Fan, M. Caleap, M. Pan, and B. W. Drinkwater, "A comparison between ultrasonic array beamforming and super resolution imaging algorithms for non-destructive evaluation," *Ultrasonics*, vol. 54, no. 7, pp. 1842–1850, 2014.

[24] C. Holmes, B. W. Drinkwater, and P. D. Wilcox, "Post-processing of the full matrix of ultrasonic transmit–receive array data for non-destructive evaluation," *NDT E Int.*, vol. 38, no. 8, pp. 701–711, 2005.

[25] M. Sutcliffe, M. Weston, B. Dutton, I. Cooper, and K. Donne, "Real-time full matrix capture with auto-focusing of known geometry through dual layered media," in *Proc. NDT Conf. Brit. Inst. Nondestruct. Test.*, 2012, pp. 1–8.

[26] R. E. Sheriff and L. P. Geldart, *Exploration Seismology*. Cambridge, U.K.: Cambridge Univ. Press, 1995.

[27] M. Sutcliffe, M. Weston, B. Dutton, I. Cooper, and K. Donne, "Real-time full matrix capture with auto-focusing of known geometry through dual layered media," in *Proc. NDT Conf. Brit. Inst. Nondestruct. Test.*, 2012, pp. 1–8.

[28] OLYMPUS. *HydroFORM/RexoFORM*. Accessed: Aug. 23, 2018. [Online]. Available: https://www.olympus-ims.com/en/corrosion-solutions/hydroform-rexoform/#!cms[tab]=%2Fcorrosion-solutions%2Fcorrosion-mapping%2Fhydroform

[29] C. Mineo, J. Riise, S. G. Pierce, P. I. Nicholson, and I. Cooper, "Robotic path planning for non-destructive testing through RoboNDT," in *Proc. 54th BINDT Annu. Conf.*, 2015.

[30] Galil. *GalilTools, Galil Motion Control*. Accessed. Aug. 16, 2018. [Online]. Available: http://www.galilmc.com/downloads/software/galiltools

[31] Peak NDT. *MicroPulse FMC*. Accessed. Aug. 16, 2018. [Online]. Available: https://www.peakndt.com/products/micropulse-fmc/

[32] TWI Ltd. (Sep. 19, 2016). *Advanced Ultrasonic Full Matrix Capture Inspection Software Launched*. Accessed: Aug. 14, 2018. [Online]. Available: https://www.twi-global.com/news-events/news/2016-09-advanced-ultrasonic-full-matrix-capture-inspection-software-launched/

[33] M. Dissanayake, T. P. Sattar, S. Lowe, I. Pinson, and T.-H. Gan, "Adaptable legged-magnetic adhesion tracked wheel robotic platform for misaligned mooring chain climbing and inspection," *Ind. Robot, Int. J.*, to be published, doi: 10.1108/IR-04-2018-0074..

**MAHESH DISSANAYAKE** (S'16) was born in Kurunegala, Sri Lanka. He received the B.Eng. degree (Hons.) (First Class) in electrical and electronic engineering from London South Bank University, U.K., in 2015, where he is currently pursuing the Ph.D. degree in robotics and mechatronics. In 2015, he joined TWI Ltd., Cambridge, U.K., as a Ph.D. Research Engineer. He is currently a Research Assistant with the London South Bank Innovation Centre. His research is focused on the development of a light-weight mobile robot for inspecting mooring chains.

**DAVE CARSWELL** received the B.Sc. degree in computer science from the University of Wales, Swansea, in 2004, and the Ph.D. degree in materials engineering (hydrodynamics of surfboard fins) in 2008. He is currently a Software Developer with TWI Ltd. He has extensive experience of computational modeling and software development in an industrial and academic context. He is a member of the British Computer Society and the Institution of Mechanical Engineers.

**MICHAEL CORSAR** received the M.Eng., M.Sc., and Ph.D. degrees. He has First Class Honors in mechanical engineering with Renewable Energy from The University of Edinburgh, and completed his post-graduate studies in turbomachinery, where he studied the design of rotating equipment. His Ph.D. involved developing a full scale tidal turbine prototype with an active load control system. He was a PI on a number of large scale experimental projects in the aerospace sector, including the development of a combustion system for a cruise missile application, validation of a novel failsafe lubrication system for civilian transport helicopter transmissions, and aerodynamic performance improvement of a multi-stage axial compressor for civil aircraft. He has also worked on projects in the energy sector developing heat recovery systems for the large reciprocating engines used in medium scale power plants. He oversaw the successful experimental validation of a new turbo-compounding system, which has recently entered the market in the EU and South America with the help from Innovate UK funding. He spent six years as the Manager of the Gas Turbine Engineering Laboratory, Cranfield University, before taking up a position as the Technical Manager of the London South Bank Innovation Centre for Robotics, NDT. In his current role, he is responsible for the delivery of nine research projects in robotics for inspection, maintenance, and repair in extreme environments.

**TARIQ PERVEZ SATTAR** received the B.Sc. degree in biology, the B.Sc. degree in electrical and electronic engineering, and the Ph.D. degree in self-tuning and adaptive control. He is a Professor at the School of Engineering, London South Bank University, London, U.K., and also the former Head of the School of Electrical, Computer and Communications Engineering. He is currently the Director and TWI Chair of the University's Innovation Centre for the Automation of Non-Destructive Testing, TWI Ltd., Cambridge, U.K. His research interests include control engineering, mechatronics, mobile robotics for inspection in extreme environments, and the integrity assessment of the safety critical infrastructure. He is a member of the Institute of Engineering and Technology, U.K., and a fellow of the British Institute of Non Destructive Testing.

**MARK SUTCLIFFE** received the Ph.D. degree in NDT (time critical synthetic transmit aperture ultrasound imaging) from the University of Wales Trinity St. David in 2015, with over 20 years of industrial experience. He is currently a Consultant (software) with TWI Ltd., specializing in novel ultrasonic data acquisition and imaging solutions. He has developed and delivered NDT inspection systems for the use in nuclear, aerospace, and space exploration. He is a Professional Member of the British Computing Society and a Chartered Engineer.

**PREMESH SHEHAN LOWE** (S'13–M'16) received the Ph.D. degree from the Electrical and Computer Engineering Department, Brunel University London, Uxbridge, U.K., in 2016. He commenced his career in the field of non-destructive testing by joining the Integrity Management Group, TWI Ltd., Cambridge, as a Research Engineer, in 2012. He joined the Brunel Innovation Centre, Cambridge, as a Research Fellow, in 2015. He is currently the Team Leader of Power Ultrasonic. His research is focused on finite element methods and signal processing on ultrasonic guided waves. He has authored or co-authored over 20 peer-reviewed journals and conferences. His research interests include ultrasonic sensor development, sound energy focusing, and fouling removal using high power ultrasonic. He has been serving as a Reviewer for the IEEE Journals, NDT&E, and *Sensors Journal* since 2014.

**TAT-HEAN GAN** received the degree in electrical and electronics engineering (Hons.) (First-Class) from the University of Nottingham, the M.Sc. degree in advanced mechanical engineering and graduated with a distinction from the University of Warwick in 1998, where he continued his Ph.D. studies in engineering, specializing in advanced ultrasonic imaging, and the Executive MBA degree from the University of Birmingham in 2006. He has worked as an academic and in industry for many years. He is an Associate Director of TWI Ltd., and the Technology Director of the National Structural Integrity Research Centre, the UK's first industry-led postgraduate education and research center in structural integrity. He is currently a Professor with Brunel University London, where he is also the Chair of the Acoustic Waves Technologies with the School of Engineering and Design. He has published over 100 papers, and has contributed to several books in the field of non-destructive testing. His research interest is in the signal and image processing, sensor development, asset integrity management, and structural assessment. He is also a fellow of the Institute of Engineering and Technology, the British Institute of Non-Destructive Testing, the International Society of Condition Monitoring, and the International Society of Engineering Asset Management. He has obtained his CEng, EurIng, and IntPE(UK) Status. He was a recipient of The Welding Institute Lidstone Award, who is deemed to have made the most significant contribution to the advancement of welding technology.